

OPEN

Coupling Chlorin e6 to the surface of Nanoscale Gas Vesicles strongly enhances their intracellular delivery and photodynamic killing of cancer cells

Ann Fernando^{1,3} & Jean Gariépy^{1,2,3*}

Protein-based nanobubbles such as halophilic archaeobacterial gas vesicles (GVs) represent a new class of stable, homogeneous nanoparticles with acoustic properties that allow them to be visualized by ultrasound (US) waves. To design GV as theranostic agents, we modified them to respond to light, with a view to locally generate reactive oxygen species that can kill cancer cells. Specifically, up to 60,000 photoreactive chlorin e6 (Ce6) molecules were chemically attached to lysine ϵ -amino groups present on the surface of each purified *Halobacterium sp.* NRC-1 GV. The resulting fluorescent NRC-1 Ce6-GVs have dimensions comparable to that of native GV and were efficiently taken up by human breast [MCF-7] and human hypopharyngeal [FaDu-GFP] cancer cells as monitored by confocal microscopy and flow cytometry. When exposed to light, internalized Ce6-GVs were 200-fold more effective on a molar basis than free Ce6 at killing cells. These results demonstrate the potential of Ce6-GVs as novel and promising nanomaterials for image-guided photodynamic therapy.

Image-guided therapies are precision medicine-based treatments being developed in many cases to treat cancer patients. These therapies benefit from the development of theranostic agents that integrate both targeted diagnostic and therapeutic functions¹⁻³.

Theranostics often incorporate radionuclides or MR contrast agents as imaging probes in conjunction with cytotoxic nuclides or drug-conjugates linked to a tumor-targeting agent such as a small ligand or an antibody that delivers the payload. An alternate design strategy to reduce potential off-target toxicities arising from delivering these agents systemically is to create theranostics that are only activated within the tumor environment (pro-drug like theranostics that become activated as a result of a local change in pH or by tumor-associated proteases) or upon exposing tumors to an external, focused energy source that would remotely activate such agents within the tumor environment only. Nanoparticles are particularly suited to this purpose as they tend to accumulate within the abnormal tumor neovasculature as a consequence of the enhanced permeability and retention (EPR) effect^{4,5}. Tumor selectivity can be encoded into nanoparticles by making them sensitive to an externally applied, ultrasound and light source; physical methods that are presently being used in image-guided therapy. Protein-based gas vesicles (GVs) represent an example of a naturally occurring nanostructure that could be used for this purpose. In the present study, we focused on GV nanostructures genetically encoded by the aquatic halophilic archaeon *Halobacterium salinarum* NRC-1⁶. They are composed of two dominant protein subunits termed gas vesicle protein A (GvpA) and gas vesicle protein C (GvpC)⁶. Due to the presence of their air-filled internal core, GV can respond to ultrasound waves and produce hyperpolarized magnetic resonance contrast for imaging^{7,8}. Moreover, as a genetically encoded nanostructure new ligands can be introduced into the surface gvpC protein through genetic recombinant approaches⁹. Alternately, GV can serve as a scaffold to incorporate new ligands or domains through chemical conjugation approaches¹⁰. In the present study, we explored the potential of such

¹Department of Pharmaceutical Sciences, The University of Toronto, 27 King's College Circle Toronto, Ontario, M5S 1A1, Canada. ²Department of Medical Biophysics, The University of Toronto, 27 King's College Circle Toronto, Ontario, M5S 1A1, Canada. ³Sunnybrook Research Institute, 2075 Bayview Ave, Toronto, ON, M4N 3M5, Canada. *email: jean.gariepy@utoronto.ca

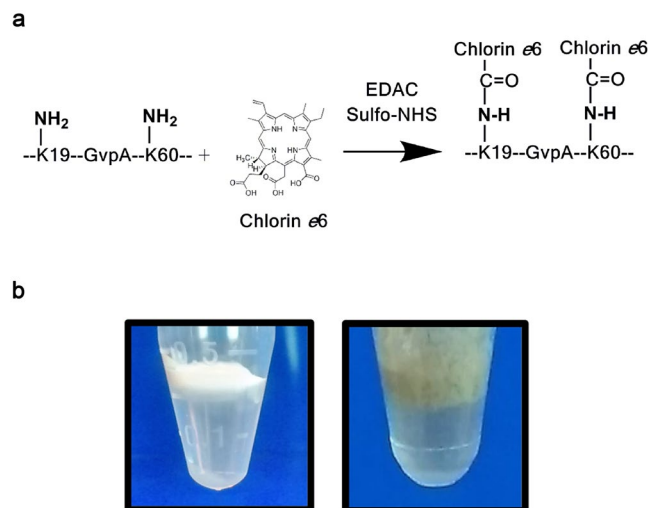


Figure 1. (a) Diagram depicting the conjugation of chlorin *e6* (Ce6) carboxylic groups to the two lysine ϵ -amino groups (K19 and K59) of GvpA, the main protein component of *Halobacterium sp. NRC-1* Gas Vesicles (GVs). (b) GV are air-filled protein nanobubbles recovered by flotation from lysed halophilic archaeobacteria. Purified floating layers are showed of wild type (WT) *Halobacterium sp. NRC-1* GV (white) and Ce6-modified GV (green-grey color).

GVs as photodynamic therapy (PDT) agents. We report the design of a light-activated GV nanoparticle where the photo-reactive dye chlorin *e6* (Ce6) was coupled to free amino groups on the surface of GV. The resulting nanoscale size structures were found to readily accumulate into cancer cells and kill them in response to light activation displaying remarkable enhancements in cytotoxicity towards cancer cells relative to free Ce6.

Results and Discussion

Preparation and characterization of GV modified with chlorin *e6* (Ce6-GV). Gas vesicles (GVs) are air-filled nanobubbles that have been shown to respond to ultrasound (US) waves⁷. Occurring in the range of 200–400 nm, GV can be exploited to image or deliver therapeutics to tumors. They are particularly advantageous over other popular nanoparticles such as liposomes or albumin-based nanoparticles because new epitopes or therapeutic ligands can be introduced at the protein subunit level by fusion to the surface gvpC protein⁹. In addition, mechanical cavitation of GV using focused ultrasound has recently been shown to mediate potent cell-killing effects, illustrating another therapeutic approach for GV¹¹. Native GV are rapidly cleared from circulation¹² and pegylation of GV has recently been reported to enhance tumor contrast imaging *in vivo*¹⁰. Combined with their facile production, inherent resilience to a range of pH and temperature conditions, and lack of toxicity, such properties present GV as a versatile and favorable nanoparticle platform to investigate for drug delivery. In this study, GV were isolated from the *Halobacterium sp. NRC-1* to serve as nanocarriers for the light-activated drug, chlorin *e6* (Ce6) with a view of creating therapeutic GV displaying features beyond their US-imaging properties. As such, NRC-1 GV were purified and their surface modified with Ce6 to demonstrate their ability to be internalized by cancer cells and to enhance the cytotoxicity of Ce6 as a photodynamic therapy (PDT) agent. Ce6-modified GV represent a first attempt at generating GV-based theranostic agents aimed at killing cancer cells. Specifically, Ce6 absorbs light with maxima observed at 400 nm and 660 nm. The photodynamic effect occurs upon absorption in the red region of the spectrum where human tissue is optically transparent, reaching tissue depth of up to 16 mm^{13,14}. Ce6 is also a fluorescent compound, which enables the use of optical imaging to detect its accumulation into tumors¹⁵.

Halobacterium sp. NRC-1 GV used in this study are composed of two major protein species (GvpA and GvpC) as well as several minor proteins involved in the nanobubble assembly. Importantly, GvpA accounts for >90% of the nanobubble structure and shell⁶. GvpC binds non-covalently to the surface of the GV shell. However, it is stripped from the nanobubble surface during the process of isolating GV from the halobacterium, as confirmed by mass spectrometry of our GV preparations (Supplementary Fig. S1). As such, the two lysine ϵ -amino groups present in GvpA (lysine 19 [helix I] and lysine 60 [helix II] of GvpA; depicted in Fig. 1a) represent the main sites for covalently attaching Ce6 to the surface of GV.

Experimentally, wild type gas vesicles (WT GV) from the *Halobacterium sp. NRC-1* were isolated by flotation from lysed halobacteria and purified by repeated centrifugation steps as described elsewhere (Fig. 1b)¹⁶. The carboxylic groups of chlorin *e6* were then activated with EDAC and sulfo-NHS to form esters that reacted with the two free ϵ -amino groups of GvpA on WT GV, resulting in an olive-green colored nanobubble preparation termed Ce6-GV (Fig. 1b).

The particle size of these GV was studied by dynamic light scattering (DLS) and transmission electron microscopy (TEM). Both WT GV and Ce6-GV adopted a characteristic prolate-spheroid, lemon-shaped structure of comparable dimensions as confirmed from electron micrographs, suggesting that decorating the surface of GV with Ce6 molecules minimally affected particle structure and size (Fig. 2, Table 1). The length of Ce6-GV along

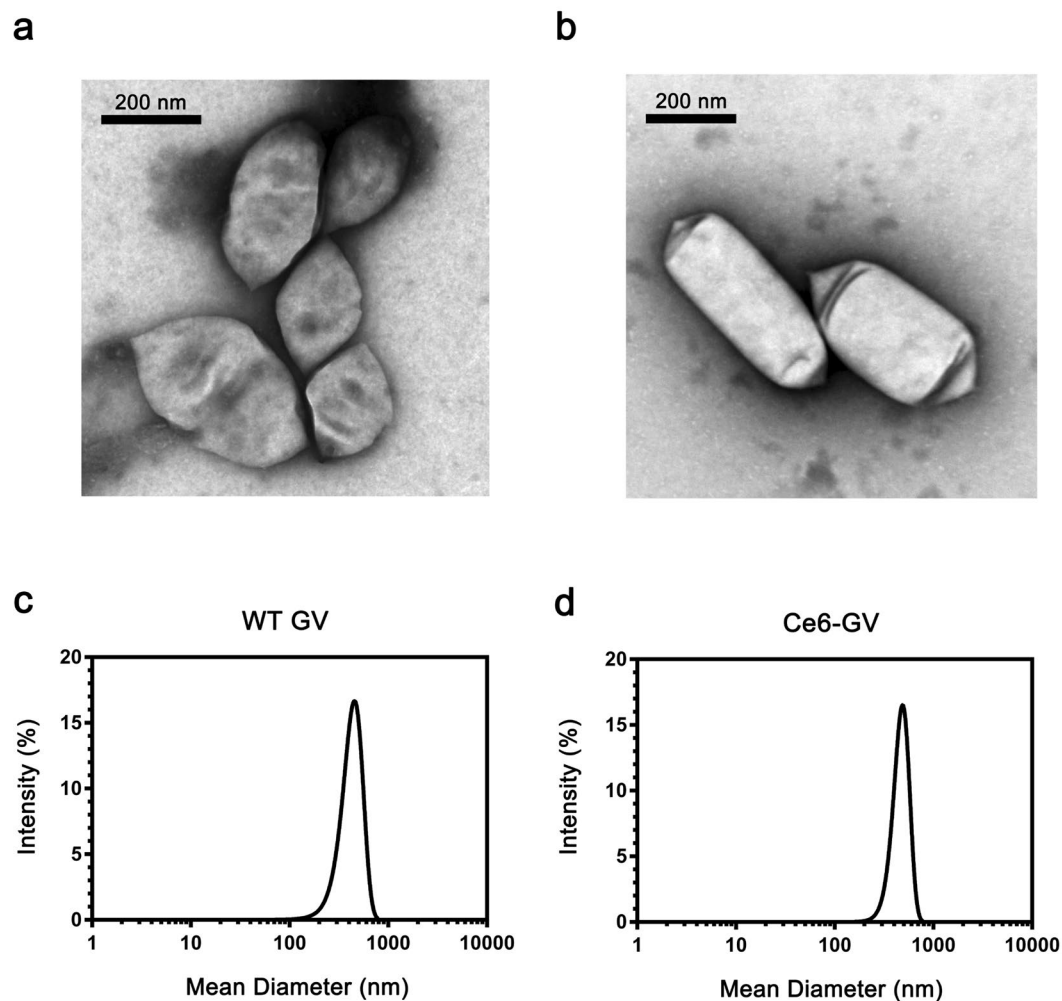


Figure 2. Characterization of WT GVs and Ce6-labeled GVs. Transmission electron micrographs of (a) WT GVs and (b) Ce6-labeled GVs indicating that modifying their surface with Ce6 yields comparable nanostructures. Similar dynamic light scattering size distribution profiles are observed for (c) WT GVs and (d) Ce6-GVs.

DLS Ce6-GV	338 ± 39 nm, n = 3
DLS WT GV	273 ± 3 nm, n = 3
TEM Ce6-GV	Length: 417 ± 109 nm, n = 3
	Width: 196 ± 38 nm, n = 3
TEM WT GV	Length: 379 ± 23 nm, n = 3
	Width: 257 ± 19 nm, n = 3
Zeta Potential Ce6-GV	-30 ± 4 mV, n = 3
Zeta Potential WT-GV	-2.4 ± 2 mV, n = 3

Table 1. Summary of size parameters for WT GVs and Ce6-GV. Results are shown as mean \pm S.D.

their long and short axes were measured to be 417 nm and 196 nm respectively according to TEM (Fig. 2, Table 1). Estimates of WT GVs and Ce6-GVs particle diameter by DLS (273 ± 3 nm and 338 ± 39 nm respectively; Table 1) assumes that GVs are spherical. The calculated diameters approximate the average length of both their short and long axes as determined by TEM (Table 1). The zeta potential of Ce6-GVs was significantly lower (-30 mV) than WT GVs (-2.4 mV) as Ce6 contains three negatively charged carboxylic acids (Table 1). The increased negative charge suggests that Ce6-GVs may have good colloidal stability due to repulsion between the nanoparticles.

Using surface area measurements of WT GVs based on TEM micrographs (Fig. 2a,b; Table 1; ~ 380 nm by 260 nm) along with the experimentally determined surface area of one GvpA molecule, the main repeating structural component of the nanobubble shell¹⁷, the mass of one *Halobacterium* GV was estimated to be 444 MDa

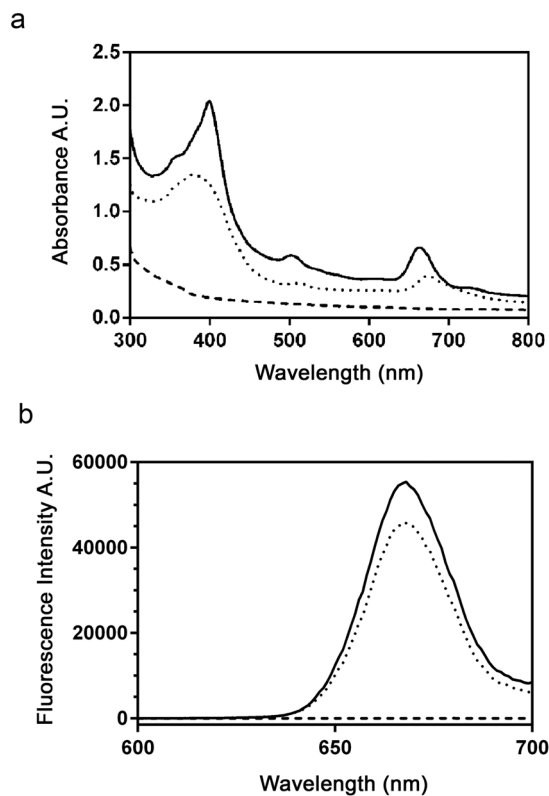


Figure 3. Absorption and Emission Spectra for Ce6-GVs. **(a)** The absorption spectrum for Ce6 released from acid-hydrolyzed Ce6-GVs was similar to that obtained for free Ce6 including peak absorption at 400 nm and 640 nm. The absorption spectrum was recorded between 300 and 800 nm in 1 nm intervals. **(b)** The fluorescence emission spectrum for Ce6 released from acid-hydrolyzed Ce6-GVs was comparable to that recorded for free Ce6. The emission spectra were recorded between 600 and 700 nm (λ_{exc} 400 nm) at 1 nm interval. The spectrum recorded for WT GV hydrolysates confirmed the absence of a Ce6 spectral signature. All spectra are representative of recordings from two independent acid-hydrolyzed samples. WT GV (broken line), Ce6-GVs (solid line), free Ce6 (dotted line).

(See Supplementary Fig. S2) with a single NRC-1 GV being composed of ~55,000 GvpA proteins. Since the two lysines present in GvpA (K19 in helix I and K60 in helix II; Fig. 1a) are projected to be solvent-accessible based on solid-state NMR¹⁸, one can project that up to 110,000 ϵ -amino groups are available to react with an amine reactive form of Ce6. To accurately determine the extent of Ce6 conjugated to WT GVs, we measured the total amount of protein (amino acid analysis) and released Ce6 content by hydrolyzing Ce6-GVs samples in 6 N HCl. It was estimated from hydrolysates that ~60,000 molecules of Ce6 molecules were coupled per nanobubble; a value representing a loading efficiency of approximately one Ce6 molecule per GypA protein.

The presence of Ce6 on GVs was further confirmed by recording the absorption and fluorescence emission spectra of Ce6-GVs (Fig. 3). The typical UV-VIS absorption spectrum of free Ce6 includes a characteristic strong absorption peak at 400 nm (Soret band) and a weaker absorption at 640 nm (Q-band)¹³. Similar absorption patterns were observed in the Ce6-GV formulation indicating successful loading of Ce6 (Fig. 3a). Moreover, the lack of absorption at these wavelengths for the native GVs was expected due to the absence of Ce6 (Fig. 3a). Similar findings were obtained for silica nanoparticles or hyperbranched-polymer composed nanoparticles covalently linked with Ce6^{13,19}. The observed fluorescence emission maximum at 660 nm recorded for Ce6-GVs was comparable to that of free Ce6, while hydrolysates from WT GVs were non-fluorescent (Fig. 3b). This finding is comparable to the published fluorescence emission spectra of equimolar doses of Ce6-liposomes and free Ce6²⁰ or Ce6-albumin nanoparticle formulations²¹. These results indicate that Ce6 can be efficiently loaded onto GVs and also demonstrate that conjugation to GVs does not significantly alter the spectral properties of Ce6, nor the shape and dimensions of GVs.

Ce6-GVs are taken up by cancer cells and accumulate in endosomes. The light-induced cytotoxicity of Ce6-containing GVs depends on their ability to be internalized by cancer cells. Upon reaching the cytoplasm and following light activation, Ce6 molecules are excited to their singlet \rightarrow triplet states where their energy can be transferred to O₂ to generate reactive singlet oxygen (¹O₂)²². Alternatively, activated Ce6 can react directly with proteins, nucleic acids and lipids to form reactive oxygen species (ROS; superoxide anion, hydroxyl radical, hydrogen peroxide) causing oxidative damage leading to cell death^{22,23}.

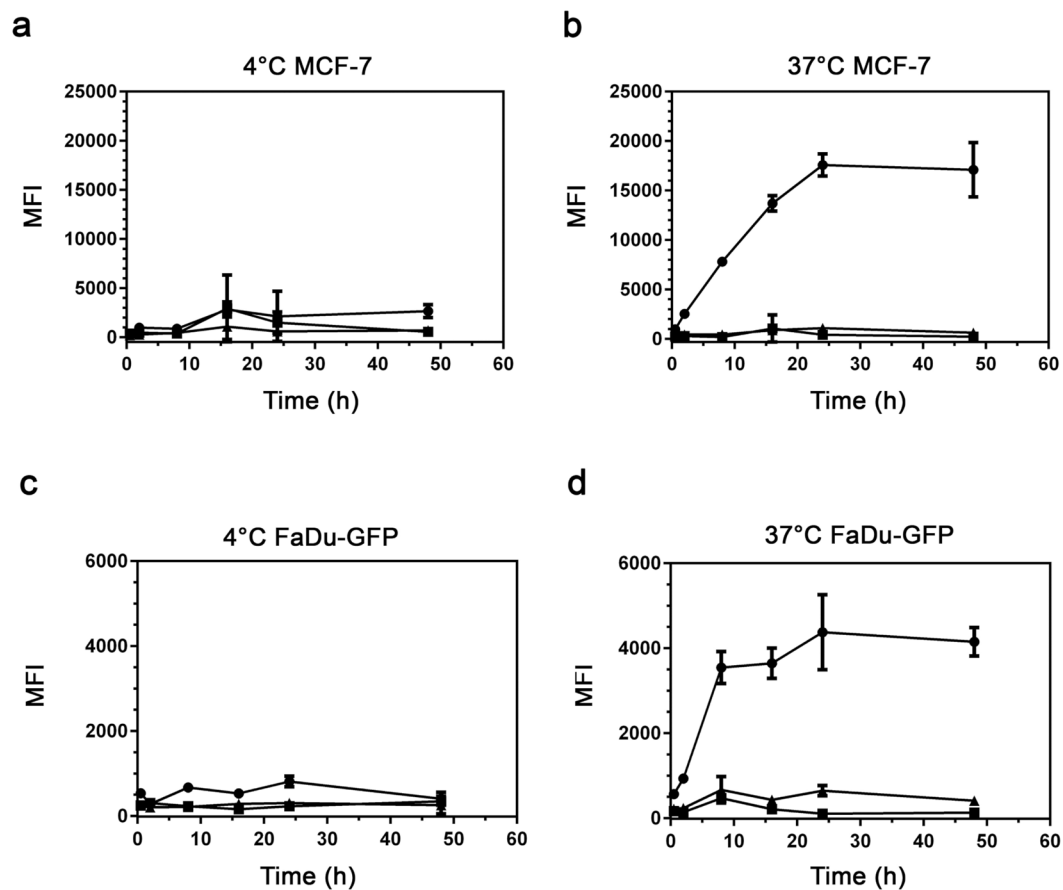


Figure 4. Mean fluorescence intensities (MFI) as determined by fluorescence-activated cell sorting (FACS) indicate that Ce6-GVs are internalized as a function of time by MCF-7 cells and FaDu-GFP cells at 37 °C (Panels b,d). In contrast, minimal cellular uptake takes place at 4 °C (Panels a,c). Cells were equivalently treated with 670 nM of Ce6 either as Ce6-GVs (closed circles) or as the free drug (closed triangles) over a 48-hour period. As projected, equivalent concentrations of WT GV (closed squares) relative to Ce6-GVs did not generate significant MFI values. Results shown are representative of two independent trials performed in triplicate and presented as averaged MFI \pm S.D. λ_{exc} 405 nm; emission Filter 660–662 nm.

The cellular uptake of Ce6-GVs, WT GV and free Ce6 by human breast carcinoma MCF-7 and human hypopharyngeal squamous cell carcinoma FaDu cells was thus assessed by flow cytometry and confocal microscopy. For both techniques, fluorescence emission signals arising from the chlorin e6 chromophore (λ_{exc} 403 nm) were captured between 660–680 nm (Fig. 3). The intracellular uptake of Ce6-GVs and free Ce6 was monitored by flow cytometry in terms of mean fluorescence intensities (MFI) as a function of time and temperature (Fig. 4). As expected, cellular uptake did not take place at 4 °C for either cell lines (Fig. 4a–c) while the internalization of Ce6-GVs at 37 °C reached a plateau at 8 hours and 22 hours for the FaDu-GFP and MCF-7 cell lines respectively (Fig. 4b–d). In contrast, free Ce6 minimally enters these cells while no fluorescence signal could be detected for WT GV (Fig. 4). These results show that conjugation of Ce6 to GVs improves the intracellular delivery of this drug into cancer cells. Cellular uptake of other Ce6 nanoparticles have been previously described as exemplified by Ce6-octalysine conjugated to superparamagnetic iron oxide nanoparticles being taken up by SKOV3 cells relative to free Ce6²⁴.

The cellular uptake of Ce6-GVs at 37 °C into MCF-7 and FaDu-GFP cells was further confirmed by confocal microscopy (Fig. 5). Specifically, a punctate pattern of Ce6 fluorescence (in red) is observed in the cytosol of these cells after an 8-hour incubation period suggesting their compartmentalization into organelles such as endosomes or vacuoles. Ce6-GVs did not reach the cell nucleus (Hoescht dye; blue color nuclei; Fig. 5a–e). This cytoplasmic distribution pattern has been observed for other Ce6-conjugates and nanoparticles^{13,25}.

Gas vesicles dramatically enhance the phototoxicity of Ce6 towards cancer cells. Human MCF-7 breast cancer and FaDu-GFP pharyngeal cancer cells were exposed to increasing concentrations of Ce6-GVs, free Ce6, or an equivalent amount of WT GV for 24 hours, followed by a 10-minute exposure to light. Their viability was assessed 24-hours later and reported as a function of the molar concentration of Ce6 being given (Fig. 6). Both cell lines remain viable in the absence of light treatment except for cells exposed to high doses of Ce6-GVs (10^{-5} M range; Fig. 6a–c). Upon light activation, cell viability was lost in a dose-dependent manner with Ce6-GV being more potent than the free drug (Fig. 6b–d). Specifically, CD_{50} values towards both cell lines

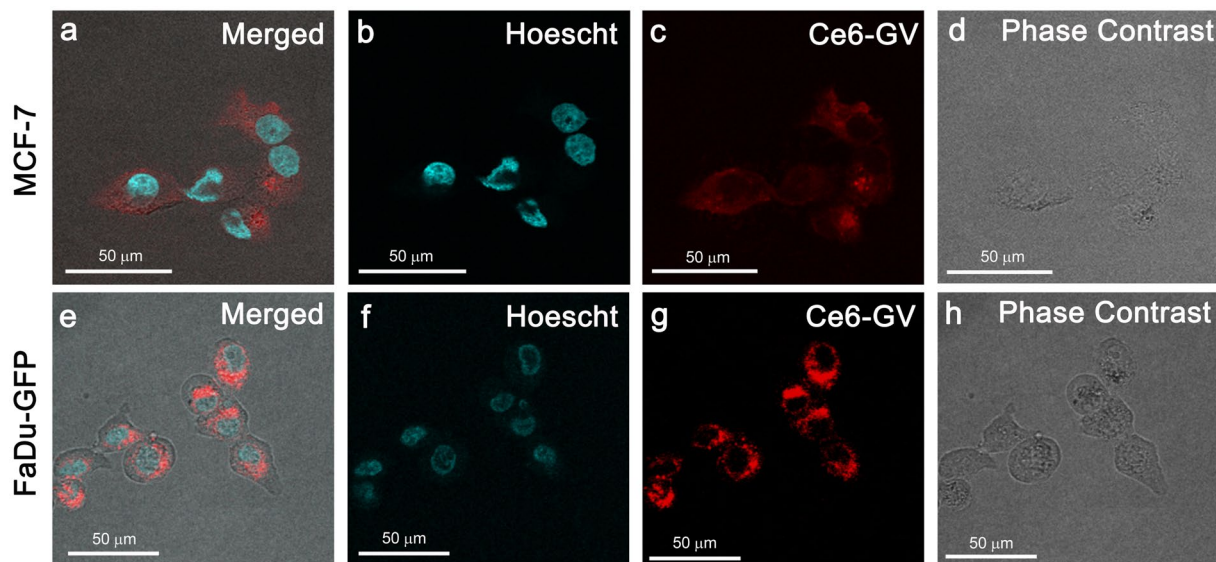


Figure 5. Merged confocal fluorescence and phase contrast microscopy images indicate that Ce6-GVs accumulate in the cytoplasm of cancer cells in a punctate-like pattern (in red) suggesting their entrapment in endocytic vesicles or vacuoles. The lack of co-localization of Ce6-GVs with the cell nucleus (Hoescht dye; blue stain) suggests that reactive oxygen species generated by Ce6-GVs being exposed to light would mainly accumulate in the cytoplasmic compartment of MCF-7 (panels a–d) or FaDu-GFP (panels e–h) cells after 8 hours of incubation.

were determined for Ce6-GV and free Ce6 (Table 2) following light exposure, with the drug covalently attached to GVs being 200-fold more toxic on a drug molar basis than free Ce6 (Fig. 6b–d). WT GVs were only toxic towards MCF-7 or FaDu-GFP at very high concentrations (at concentrations $>10^{-4}$ M relative to comparable Ce6-GV doses given; Supplementary Fig. S3). The enhanced toxicity observed for Ce6-GV correlates with its greater cellular uptake seen in both cell lines in contrast to free Ce6 (Figs. 4 and 5).

This enhancement in light-activated toxicity relative to the free form of the drug has been observed in SKOV3 and MDA-MB-231 cells for other Ce6-nanoparticles such as Ce6-SPION²⁴ or Ce6-conjugated poly(ethylene glycol)-poly-(d,l-lactide)²⁶ nanoparticles, likely owing to their improved cellular uptake. Although the level of cell killing enhancement with nanostructures modified or carrying chlorin *e6* is rarely reported relative to the free drug itself, they are examples where one can approximate the enhancement factor. For instance, self-assembled protein-based nanoparticles (50–200 nm) composed of matrix metalloproteinase polypeptides modified with Ce6 were modestly more phototoxic (2.3 fold) at the equivalent molar dose of 4.2 μ M compared to free Ce6²⁷. In the case of chlorin *e6*-encapsulated polyphosphoester nanocarriers (44 nm particles), it was demonstrated that these nanoparticles resulted in a 75% drop in BxPC-3 pancreatic cancer cell viability as compared to free Ce6 given at a single molar concentration of Ce6 where these cells were mostly viable²⁸. In the case of hyperbranched polymer-based Ce6 nanoparticles, it was reported that such particles were approximately ten-fold more toxic than free Ce6 on a molar basis¹⁹. However, cell viability was assessed after only four hours of treatment and following a three-minute light irradiation period as compared to Ce6-GV (twenty-four hours treatment with ten minutes of irradiance). These differences may explain variations in enhanced toxicity between formulations. Similarly, at an equivalent Ce6 dose of 1 μ M, dextran nano-photosensitizers bearing Ce6 improved phototoxicity by a factor of 5 relative to free Ce6 as determined with MTT assay towards HCT116 colon cancer cells²⁹. Again, the phototoxic enhancement of Ce6-GV relative to free Ce6 reported here is still superior to this dextran formulation by a factor of 40. This difference in enhancement may simply reflect the fact that cells were treated for only 2 hours with these Ce6 modified dextran nanoparticles. Surprisingly, the photosensitizing efficacy and toxicity of a Ce6-conjugated human serum albumin nanoparticle were comparable to that of free Ce6³⁰ suggesting that all Ce6-nanoparticle formulations are not equivalent in terms of enhanced cytotoxicity. In summary, Ce6-GVs are particularly effective at enhancing the killing of cancer cells in vitro relative to most reported Ce6-modified nanoparticles.

Interestingly, agents such as Ce6 can also be activated by ultrasound waves; an approach termed sonodynamic therapy that may allow one to target deep-seated tumors following the activation of the photosensitizer agent³¹. For example, the viability of H22 hepatocellular carcinoma cells exposed to 50 μ g/ml of free Ce6 for 4 hours was decreased by 40% following ultrasound treatment³². Although ultrasound is a less potent activation modality than light, our present study now suggests that the use of Ce6-GVs rather than free Ce6 may address this limitation. As such, Ce6-GVs are now being assessed as a new class of sono-sensitive agents.

The enhanced toxicity of Ce6-GVs towards cells is mechanistically related to their cellular accumulation and the production of intracellular ROS. The phototoxic effect of Ce6 is related to the production of intracellular reactive oxygen species (ROS) as a consequence of the drug being exposed to light. This effect was measured by treating cells with the green fluorescence-emitting probe, DCFH-DA, prior

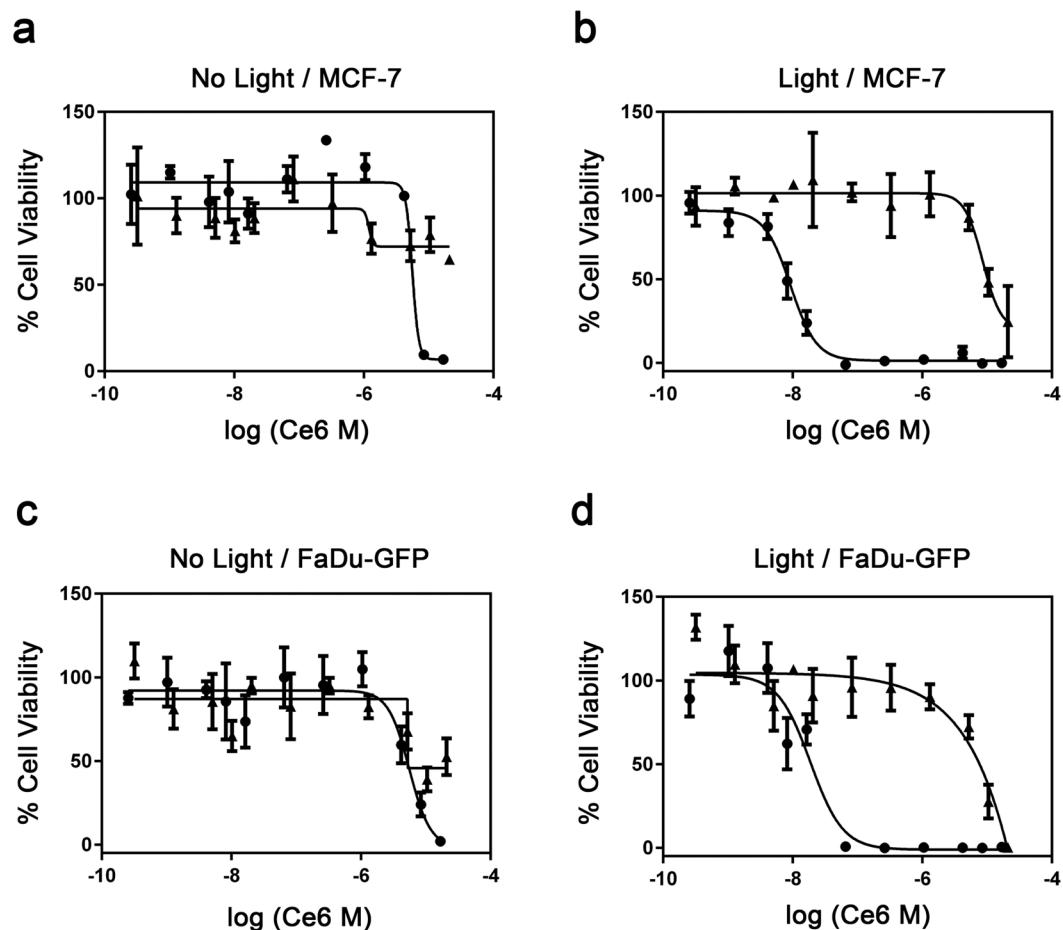


Figure 6. Dose-dependent cell viability study of MCF-7 cells or FaDu-GFP cells treated with free Ce6 (closed triangles) or Ce6-GVs (closed circles) and exposed (Panels b,d) or not (Panels a,c) to light as determined using the WST-1 cell viability assay. Results are shown as mean \pm S.D. $n = 3$ from 2 independent experiments, with each concentration performed in triplicate.

	MCF-7 CD ₅₀ (M)	FaDu-GFP CD ₅₀ (M)
Ce6-GV	$2.6 \pm 1.4 \times 10^{-8}$	$2.4 \pm 0.8 \times 10^{-8}$
Free Ce6	$5.3 \pm 3.3 \times 10^{-6}$	$5.5 \pm 4.0 \times 10^{-6}$
Free Ce6 CD ₅₀ / Ce6-GV CD ₅₀	204	229

Table 2. Comparison of CD₅₀ values determined for MCF-7 cells and FaDu-GFP cell lines following their exposure to free Ce6 and Ce6-GV. Molarity was calculated based on the molar concentration of Ce6.

to illumination. As presented in Fig. 7, the DCFH-DA fluorescence emission signal for MCF-7 and FaDu-GFP treated with Ce6-GV confirm the presence of ROS in light-treated cells only (Fig. 7a,b). For MCF-7 and FaDu-GFP cell lines, significantly more ROS were produced when Ce6-GV-loaded cells were exposed to light as compared to Ce6-GV-loaded cells kept in the dark ($p = 0.0052$ and $p = 0.0004$ respectively). The difference in ROS production due to Ce6-GV treatment was greater than ROS production due to free Ce6 treatment in either MCF-7 ($p = 0.0385$) or FaDu-GFP cell lines ($p = 0.0126$). These results confirm that conjugating Ce6 to GVs does not impair their capacity to produce ROS and is consistent with the superior uptake of Ce6-GV relative to free Ce6 demonstrated by flow cytometry (Fig. 4). Internalization events favoring the accumulation of Ce6-GVs over the free drug inside cells probably play a dominant role in enhancing the toxicity of Ce6 towards cancer cells. The generation of ROS is expected to cause damage to intracellular components such as protein, DNA, or membranes and trigger apoptotic or necrotic pathways to mediate cell death³³. In the case of Ce6-GVs, confocal images presented in Fig. 5 suggest that these nanobubbles never reach the cell nucleus indicating that the generated reactive oxygen species following illumination are mainly deposited in the cytoplasm of these cells, preferentially causing the oxidation of lipids and proteins rather than damaging nucleic acid species^{34,35}.

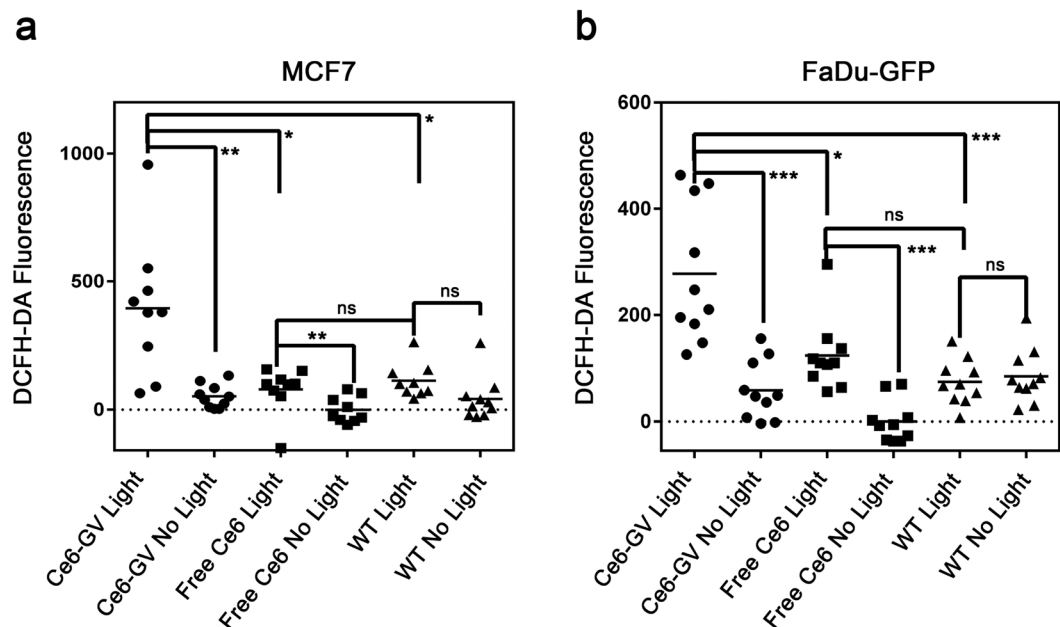


Figure 7. Production of Reactive Oxygen Species (ROS) in MCF-7 and FaDu-GFP cells treated with Ce6-GV, WT GV, or free Ce6. The ROS-sensitive probe DCFH-DA was subsequently loaded into treated cells with or without light activation of Ce6. ROS levels were quantified using a fluorescence plate reader. The results are shown as mean \pm S.D. ($n = 10$). Statistical significance was determined with a paired t-test, $p < 0.05^*$, $p < 0.01^{**}$, $p < 0.001^{***}$, $p < 0.0001^{****}$.

Conclusions

We have covalently linked the photoreactive drug Ce6 to nanoscale gas vesicles (GVs) with a view to expand their potential as nanoparticles responding to ultrasound waves and now to light. This newly-introduced function suggests that GV's represent a good platform for designing stable theranostic agents that can be externally activated to serve as both imaging and now as locally-activated therapeutic agents. Specifically, Ce6-GVs were efficiently internalized by MCF-7 and FaDu-GFP cancer cells and were highly effective in killing them *in vitro* upon light activation, relative to the free drug.

Material and Methods

Production and purification of gas vesicles. Gas vesicles were isolated from *Halobacterium sp. NRC-1*. Cells were cultured in CM+ growth medium [4.3 M sodium chloride, 81 mM magnesium sulfate heptahydrate, 10 mM trisodium citrate dehydrate, 27 mM potassium chloride, 0.5% casein hydrolysate (Sigma), 0.3% yeast extract (Difco)] at 42°C, shaking at 100 rpm for one week until cells were confluent. The cultures were subsequently transferred to sterile separatory funnels and the fraction of cells expressing GV's at a high level were allowed to accumulate at the top by flotation over a one-week period. GV's were collected by hypotonic lysis of the buoyant cell fraction using 1 mM MgSO₄ solution. After lysis, GV's were purified using repeated centrifugation steps at 300 g overnight for at least three days and washed with PBS at each step. Intact buoyant vesicles were re-suspended in PBS and dialyzed against PBS (100 kDa MWCO dialysis membrane; Biotech CE) as a final step.

Fabrication of chlorin e6-decorated GV's. A mixture of chlorin e6 (Ce6; 119 μ g, Cayman Chemicals, 20 mM), 1-1-(3-di-methylaminopropyl)-3-ethylcarbodiimide hydrochloride (EDAC) (116 μ g, 60 mM) prepared in PBS) and sulfo-N-hydroxysuccinimide (sulfo-NHS) (132 μ g, 60 mM) dissolved in a volume of 10 μ L DMF was rotated for 3 hours at 25°C in the dark, in order to activate the three carboxyl groups of Ce6. Briefly, the amount of Ce6 used corresponded to a 1000-fold molar excess of this agent relative to the available amino groups present in 800 μ g of GV's. Separately, 50 μ L of DMF was added to 800 μ g of GV's suspended in 60 μ L of PBS at pH 7. The activated Ce6 solution (10 μ L) was then added to the GV suspension and the final mixture was rotated for 5 hours in the dark at 25°C. The nanoparticles were subsequently separated by centrifugation (300 g, 25°C) and washed with PBS to remove residual free Ce6. The grey-colored, Ce6-modified GV suspension was stored at 4°C in PBS.

Determination of Ce6 loading on GV's. The amino acid composition and protein concentration of the Ce6-GV preparation were accurately determined by amino acid hydrolysis (Hospital For Sick Children Toronto, CA). Ce6-GV samples were also hydrolyzed (110°C in 6N HCl *in vacuo*) to release Ce6 covalently bound to lysine ϵ -amino groups on the surface of GV's. The concentration of Ce6 released from Ce6-GV sample hydrolysates was determined by fluorescence spectroscopy using a free Ce6 standard curve (λ_{exc} 400 nm; λ_{em} 660 nm; see Supplementary Fig. S4).

Nanoparticle characterization. The shape and size of intact Ce6-GVs were established by transmission electron microscopy (Phillips/FEI Tecnai Hillsboro OR) and by dynamic light scattering (Zetasizer Nano ZS, Malvern, UK). The size distribution of Ce6-GVs derived from electron micrographs was estimated using ImageJ software³⁶. Absorption and emission spectra of Ce6-GVs were recorded using a fluorescence microplate reader (Synergy H1) at a concentration of 1.9 μM of Ce6 in the form of free Ce6 or Ce6-GV or the equivalent amount of WT GV. The Zeta potential of Ce6-GV or WT GV nanoparticles (final concentration of 40 pM in 990 μL of distilled water) was determined using the Zetasizer Nano ZS (Malvern, UK).

Cellular uptake studies. For cellular studies, the human breast cancer cell line MCF-7 was purchased from ATCC (cat.# HTB-22). The human hypopharyngeal cancer cell line FaDu-GFP (AntiCancer Inc., San Diego, CA) was a gift from Dr. David Goertz (Sunnybrook Research Institute, Toronto). MCF-7 and FaDu-GFP cells (10^6 cells) were seeded into wells of 12-well plates and incubated overnight (37°C, 5% CO₂) to enable cell attachment. Ce6-GVs, free Ce6 (both adjusted to 670 nM Ce6) or native GVs (equivalent to the Ce6-GV concentration) were dispensed into wells. Plates were then kept rotating at 4°C or 37°C in an incubator with cells being collected over time [0.5 to 48 hours] to assess their viability and the internalization of Ce6 and GVs. Briefly, cells were trypsinized and washed with PBS once. Cellular uptake of Ce6 as a function of incubation time was measured by flow cytometry as mean fluorescence intensities (MFI); λ_{exc} 405 nm, BP Filter 660–2 nm, Dichroic 635LP; LSR II, BD Biosciences, San Jose, CA). Internalization events of Ce6 and Ce6-GVs in MCF-7 or FaDu-GFP cells were also recorded by confocal microscopy. Specifically, MCF-7 or FaDu-GFP cells were seeded into an 8-well confocal chamber at a density of 10^5 cells for 24 h (37°C, 5% CO₂). The cells were then treated with Ce6-GV, free Ce6, or an equivalent amount of WT GV for 8 hours. Cell nuclei were stained using the cell permeable dye Hoescht 33342 (1 μM ; ThermoFischer). Cells were then washed with PBS and both phase contrast and fluorescence (λ_{exc} 403 nm, λ_{em} 663–738 nm) images captured using a Nikon A1 laser-scanning microscope.

Cell viability measurements. The cytotoxicity of Ce6-GV, free Ce6, or WT GV towards MCF-7 human breast cancer and FaDu-GFP pharyngeal cancer cell lines was assessed using the tetrazolium salt-based WST-1 cell proliferation assay. Briefly, cells were seeded at an initial density of 10^5 cells and were incubated overnight (37°C, 5% CO₂) to enable attachment. The next day, cells were treated for 24 hours with serial dilutions of either Ce6-GVs, equivalent molar doses of free Ce6, or corresponding amounts of native GVs relative to Ce6-GVs. Cells were subsequently washed once with PBS and exposed to a LED light source (660 nm) for 10 min (ABI 25 W Deep Red). The source irradiance was determined to be 15–35 mW/cm² (Newport Powermeter 1918-R). The plate containing Ce6-GV, free Ce6, or WT GV-treated cells not exposed to the light source served as a control for non-light associated cytotoxicities. Following light exposure, cells were incubated for an additional 24 hours in the dark. After this period, media was discarded and cells were incubated with 10 μL of WST-1 reagent (Roche) and 90 μL of growth medium for 4 hours. Absorbance readings at 480 nm were then recorded using a microplate reader (Synergy H1). Cell viability was normalized relative to a positive control (50 $\mu\text{g}/\text{mL}$ Doxorubicin-HCl treatment leading to complete cell death) and a negative control (untreated cells) using the following equation:

$$\frac{((\text{Absorbance}_{\text{sample}} - \text{Absorbance}_{\text{positive control}})/(\text{Absorbance}_{\text{negative control}} - \text{Absorbance}_{\text{positive control}})) \times 100\%}{(1)}$$

Two independent trials were performed and each data point represents the average cell survival percentage ($\pm\text{SD}$) derived from proliferation assays performed in triplicate for each tested treatment.

Detection of intracellular reactive oxygen species (ROS). 2,7-Dichlorofluorescein diacetate (DCF-DA) (Sigma) is a non-fluorescent, cell-permeable probe used to measure intracellular ROS. DCF-DA is deacetylated by intracellular enzymes to a non-fluorescent dye that is finally oxidized by ROS to the fluorescent compound dichlorofluorescein³⁷. For this assay, MCF-7 or FaDu-GFP cells were seeded into 24-well plates (5×10^5 cells) overnight and were subsequently treated for 8 hours with Ce6-GV, free Ce6 (based on a molar concentration equivalent of 500 nM) or WT GV (at a dose identical to that of Ce6-GV) to allow for their internalization. Cells were then washed with PBS and the plates were either exposed to light (660 nm) for 10 min or kept in the dark. After the light treatment, 2.5 μL of 1 mM DCF-DA dissolved in DMSO (5 μM final concentration in wells) was dispensed into each well and left for 30 min at 37°C in an incubator. Cells were washed twice under dark conditions with PBS and the DCF fluorescence emission signal was recorded using a micro-plate reader (λ_{exc} 488 nm; λ_{em} 525 nm) (Synergy H1). The fluorescence emission values were normalized relative to the average DCF fluorescence of cells treated with free Ce6 in the absence of light. The results were analyzed with a one-tailed paired t-test to evaluate the difference between paired groups based on sample size of $n = 10$. Significant differences were determined as $\alpha < 0.05$. Normality of the data distribution was confirmed using Kolmogorov-Smirnov test.

Data availability

Data is available upon reasonable request from the corresponding author.

Received: 6 August 2019; Accepted: 27 January 2020;

Published: 18 February 2020

References

- Warner, S. Diagnostics + Therapy = Theranostics. *The Scientist Magazine*[®]. Available at, <https://www.the-scientist.com/profession/diagnostics-therapy-theranostics-49660> [Accessed 26 Apr. 2019] (2019)
- Taber, S. W., Fingar, V. H., Coots, C. T. & Wieman, T. J. Photodynamic Therapy Using Mono-L-Aspartyl Chlorin E6 (Npe6) for the Treatment Of Cutaneous Disease: A Phase I Clinical Study. *Clin. Cancer Res.* **4**, 2741–2746 (1998).
- Baum, R. P. & Kulkarni, H. R. Theranostics: From Molecular Imaging Using Ga-68 Labeled Tracers And PET/CT To Personalized Radionuclide Therapy—The Bad Berka Experience. *Theranostics.* **2**, 437–447 (2012).

4. Matsumura, Y. & Maeda, H. A New Concept For Macromolecular Therapeutics In Chemotherapy: Mechanism Of Tumoritrophic Accumulation Of Proteins And The Antitumor Agent Smancs. *Cancer Res.* **12**, 6387–92 (1986).
5. Greish, K. Enhanced Permeability and Retention (EPR) Effect for Anticancer Nanomedicine Drug Targeting. *Methods Mol. Biol.* 25–37 (2010).
6. Walsby, A. E. Gas Vesicles. *Microbiol. Rev.* **58**, 94–144 (1994).
7. Shapiro, M. *et al.* Biogenic Gas Nanostructures As Ultrasonic Molecular Reporters. *Nat. Nanotechnol.* **9**, 311–316 (2014).
8. Kunth, M., Lu, G., Witte, C., Shapiro, M. & Schröder, L. Protein Nanostructures Produce Self-Adjusting Hyperpolarized Magnetic Resonance Imaging Contrast through Physical Gas Partitioning. *ACS Nano.* **12**, 10939–10948 (2018).
9. Sremac, M. & Stuart, E. S. Recombinant gas vesicles from *Halobacterium* sp. displaying SIV peptides demonstrate biotechnology potential as a pathogen peptide delivery vehicle. *BMC Biotechnol.* **8** (2008).
10. Yan, J., Yin, M., Foster, F. & Démoré, C. Tumor Contrast Imaging with Gas Vesicles by Circumventing the Reticuloendothelial System. *Ultrasound in Med. Biol.* (2019).
11. Bar-Zion, A. *et al.* Acoustically Detonated Biomolecules for Genetically Encodable Inertial Cavitation. bioRxiv **620567**; <https://doi.org/10.1101/620567> (2019).
12. Le Floch, J. *et al.* In Vivo Biodistribution Of Radiolabeled Acoustic Protein Nanostructures. *Mol. Imaging Biology.* **20**, 230–239 (2018).
13. Bharathiraja, S. *et al.* Chlorin e6 Conjugated Silica Nanoparticles for Targeted and Effective Photodynamic Therapy. *Photodiagnosis Photodyn. Ther.* **19**, 212–220 (2017).
14. Kostenich, G., Zhuravkin, I., Furmanchuk, A. & Zhavrid, E. Photodynamic Therapy With Chlorin E6. A Morphologic Study Of Tumor Damage Efficiency In Experiment. *J. Photochem. Photobiol.* **11**, 307–318 (1991).
15. Chin, W. W. *et al.* In-Vivo Optical Detection of Cancer Using Chlorin e6 – Polyvinylpyrrolidone Induced Fluorescence Imaging and Spectroscopy. *BMC Medical Imaging.* **9** (2009).
16. Lakshmanan, A. *et al.* Preparation Of Biogenic Gas Vesicle Nanostructures For Use As Contrast Agents For Ultrasound And MRI. *Nat. Protoc.* **12**, 2050–2080 (2017).
17. Blaurock, A. E. & Walsby, A. E. Crystalline Structure of the Gas Vesicle Wall from *Anabaena Flos-Aquae*. *J. Mol. Biol.* **105**, 183–199 (1976).
18. Strunk, T. *et al.* Structural Model of the Gas Vesicle Protein GvpA and Analysis of GvpA Mutants *in Vivo*. *Mol. Microbiol.* **81**, 56–68 (2011).
19. Li, P. *et al.* Photodynamic therapy with hyperbranched poly(ether-ester) chlorin(e6) nanoparticles on human tongue carcinoma CAL-27 cells. *Photodiagn Photodyn.* **9**, 76–82 (2012).
20. Antonenko, Y. *et al.* Photodynamic Activity Of The Boronated Chlorin E6 Amide In Artificial And Cellular Membranes. *Biochim. Biophys. Acta – Biomembr.* **1838**, 793–801 (2014).
21. Shton, I., Sarnatskaya, V., Prokopenko, L. & Gamaleia, N. Chlorin e6 Combined With Albumin Nanoparticles As A Potential Composite Photosensitizer For Photodynamic Therapy Of Tumors. *Exp. Oncol.* **37**, 250–254 (2015).
22. Master, A., Livingston, M. & Sen Gupta, A. Photodynamic Nanomedicine in the Treatment of Solid Tumors: Perspectives and Challenges. *J. Control. Rel.* **168**, 88–102 (2013).
23. Kostryukova, L., Prozorovskiy, V., Medvedeva, N. & Ipatova, O. Comparison Of A New Nanoform Of The Photosensitizer Chlorin e6, Based On Plant Phospholipids, With Its Free Form. *FEBS Open. Bio.* **8**, 201–210 (2018).
24. Zhao, L. *et al.* Efficient Delivery Of Chlorin E6 Into Ovarian Cancer Cells With Octylsine Conjugated Superparamagnetic Iron Oxide Nanoparticles For Effective Photodynamic Therapy. *J. Mater. Chem. B.* **4**, 7741–7748 (2016).
25. Yaghini, E. *et al.* Endolysosomal Targeting of a Clinical Chlorin Photosensitizer for Light-Triggered Delivery of Nano-Sized Medicines. *Sci. Rep.* **7** (2017).
26. Kumari, P., Rompicharla, S., Bhatt, H., Ghosh, B. & Biswas, S. Development Of Chlorin E6-Conjugated Poly(Ethylene Glycol)-Poly(D,L-Lactide) Nanoparticles For Photodynamic Therapy. *Nanomedicine.* **14**, 819–834 (2019).
27. Hou, W. *et al.* MMP2-Targeting and Redox-Responsive PEGylated Chlorin e6 Nanoparticles for Cancer Near-Infrared Imaging and Photodynamic Therapy. *ACS Appl. Mater. Interfaces.* **8**, 1447–1457 (2016).
28. Ding, F. *et al.* Chlorin e6-Encapsulated Polyphosphoester Based Nanocarriers with Viscous Flow Core for Effective Treatment of Pancreatic Cancer. *ACS Appl. Mater. Interfaces.* **7**, 18856–18865 (2015).
29. Chu, C. *et al.* Redox-Responsive Nanophotosensitizer Composed of Chlorin e6-Conjugated Dextran for Photodynamic Treatment of Colon Cancer Cells. *J. Nanomater.* **2016**, 1–12 (2016).
30. Jeong, H. *et al.* Photosensitizer-Conjugated Human Serum Albumin Nanoparticles for Effective Photodynamic Therapy. *Theranostics* **1**, 230–23 (2011).
31. Umemura, S., Yumita, N., Nishigaki, R. & Umemura, K. Mechanism Of Cell Damage By Ultrasound In Combination With Hematoporphyrin. *Jpn. J. Cancer Res.* **81**, 962–966 (1990).
32. Zhang, P. *et al.* Iron Oxide Nanoparticles As Nanocarriers To Improve Chlorin E6-Based Sonosensitivity In Sonodynamic Therapy. *Drug. Des. Devel. Ther.* **12**, 4207–4216 (2018).
33. Kimura, H. *et al.* Toxicity and Roles of Reactive Oxygen Species. *Curr. Drug. Target. Inflamm. Allergy.* **4**, 489–495 (2005).
34. Sakharov, D. V., Elstak, E. D. R., Chernyak, B. & Wirtz, K. W. A. Prolonged Lipid Oxidation After Photodynamic Treatment. Study With Oxidation-Sensitive Probe C11-Bodipy 581/591. *FEBS Lett.* **579**, 1255–1260 (2005).
35. Szokalska, A. *et al.* Proteasome Inhibition Potentiates Antitumor Effects Of Photodynamic Therapy In Mice Through Induction Of Endoplasmic Reticulum Stress And Unfolded Protein Response. *Canc. Res.* **69**, 4235–4243 (2009).
36. Schneider, C. A., Rasband, W. S. & Eliceiri, K. W. NIH Image to ImageJ: 25 years of Image Analysis. *Nat. Methods.* **9**, 671–675 (2012).
37. Chen, X., Zhong, Z., Xu, Z., Chen, L. & Wang, Y. 2',7'-Dichlorodihydrofluorescein as a Fluorescent Probe for Reactive Oxygen Species Measurement: Forty Years of Application and Controversy. *Free. Radic. Res.* **44**, 587–604 (2010).

Acknowledgements

We would like to thank Dr. Gang Zheng (University of Toronto) for critically reviewing this manuscript and Dr. Christine Allen (University of Toronto) for her support with this project. This study was supported by a grant from the Canadian Institutes of Health Research to J.G.

Author contributions

A.F. designed the experiments with advice from J.G. A.F. performed the experiments, analyzed the results, and prepared the manuscript. The manuscript was revised by J.G.

Competing interests

The authors declare no competing interests.

Additional information

Supplementary information is available for this paper at <https://doi.org/10.1038/s41598-020-59584-1>.

Correspondence and requests for materials should be addressed to J.G.

Reprints and permissions information is available at www.nature.com/reprints.

Publisher's note Springer Nature remains neutral with regard to jurisdictional claims in published maps and institutional affiliations.



Open Access This article is licensed under a Creative Commons Attribution 4.0 International License, which permits use, sharing, adaptation, distribution and reproduction in any medium or format, as long as you give appropriate credit to the original author(s) and the source, provide a link to the Creative Commons license, and indicate if changes were made. The images or other third party material in this article are included in the article's Creative Commons license, unless indicated otherwise in a credit line to the material. If material is not included in the article's Creative Commons license and your intended use is not permitted by statutory regulation or exceeds the permitted use, you will need to obtain permission directly from the copyright holder. To view a copy of this license, visit <http://creativecommons.org/licenses/by/4.0/>.

© The Author(s) 2020